Pergamon

PII: S0148-9062(96)00066-6

Int. J. Rock Mech. Min. Sci. Vol. 34, No. 5, pp. 805–816, 1997

Printed in Great Britain
0148-9062/97 $17.00 + 0.00

The Influence of Grain Size and Porosity on Crack Initiation Stress and Critical Flaw Length in Dolomites

Y. H. HATZOR†
V. PALCHIK†

The influence of rock texture on crack initiation stress (σ_i) and critical flaw length (L_i) is studied by a series of triaxial tests performed on monomineralic dolomites. The critical flaw length, as predicted by analytical models, is shown to be larger than the measured mean grain size (d_m) by two–three orders of magnitude. This discrepancy is explained by rock texture variations, which influence the fracture propagation mode and consequently fracture initiation stress. The quantification of rock texture is accomplished using porosity. Fracture initiation stress is shown to be inversely related to both porosity and mean grain size. When porosity is low, the sensitivity of σ_i to mean grain size is high. This effect is reduced with higher porosity values. A model for initial flaw length is developed by a synthesis of Griffith initiation criteria with our empirical model for fracture initiation stress. Initial flaw length is found to be directly proportional to the elastic modulus, mean grain size and porosity of the rock. When porosity and mean grain size decrease simultaneously, the initial flaw length rapidly decreases and approaches the mean grain size value. Therefore, the classical assumption that grain size scales initial flaw size is shown to be valid only in the very restricted case of low porosity–low grain size rocks. In such textures, where void space is minimal, available crystal faces function as truly initial flaws, and variations in mean grain size influence crack initiation stress significantly. In more porous textures, however, the initial flaw length is shown to be up to two orders of magnitude higher than the mean grain size in the rock, depending upon the porosity and mean grain size values. In such textures crack initiation stress is much less sensitive to variations in mean grain size, indicating that the role of individual grains is less significant. © 1997 *Elsevier Science Ltd*

INTRODUCTION

The influence of grain size on rock strength has been studied by several authors. Hugman and Friedman [1] have shown that ultimate strength is inversely proportional to mean grain size in carbonate rocks such as limestones and dolomites. This has also been observed by Olsson [2] who has shown that the stress difference at failure is linearly proportional to the inverse square root of the mean grain size ($d^{-1/2}$) in marbles. Olsson [2] has suggested that Petch theory on the relation between yield stress and grain size in metals [3] is also valid in polycrystalline aggregates, such as carbonate rocks. Fredrich *et al.* [4] confirmed a Hall–Petch relation in a variety of carbonate rocks of varying mean grain size values.

The fracture initiation mechanism that has been assumed in experimental work on sedimentary rocks has been the sliding crack model [4, 5], for which analytical solutions are available [6, 7]. The working hypothesis in these studies is that grain boundaries function as potential Griffith flaws in the material. With application of the remote compressive stress, stress concentrations develop at the tip of the flaws, and maximum concentrations evolve at the tip of cracks which are inclined at a critical angle with respect to the principal

†Rock Mechanics Laboratory of the Negev, Department of Geology and Mineralogy, Ben-Gurion University of the Negev, Beer-Sheva, 84105, Israel.

compressive stress axis. The general form of stress concentration for any fracture mode is given by:

$$K = Y\sigma\sqrt{\pi a} \tag{1}$$

where K is the stress intensity factor, Y is a numerical modification factor to account for crack geometry, loading conditions and edge effets, and a is the half crack length [8]. The critical stress intensity factor (K_{IC}) at crack initiation was derived by Ashby and Hallam [7] for the sliding crack model. Assuming mode I fracture propagation in an infinite homogeneous and continuous plate containing a single crack, K_{IC} is found by seeking the plane on which the tensile stress is a maximum:

$$\frac{\sigma_1\sqrt{\pi a}}{K_{IC}} = \frac{-\sqrt{3}}{[(1-\lambda)\sqrt{1+\mu^2}-(1+\lambda)\mu]} \tag{2}$$

where σ_1 is the major principal compressive stress required for fracture initiation, $\lambda = \sigma_1/\sigma_3$ (principal stress ratio), and μ is the coefficient of friction. The solution is identical with that of Nemat-Nasser and Horii [6], and similar in form to the solution of McClintock and Walsh [9]. The equation is strictly valid when the remote stress σ_1 is compressive because in tension the frictional component disappears.

An experimental method for detecting crack initiation stress has been discussed by Martin and Chandler [10]. They have argued that the volumetric strain measured by three orthogonal strain gages, aligned in parallel with the principal stress axes during deviator stress application, are total volumetric strains, which include both elastic and inelastic volumetric strain components. The elastic volumetric strain in a conventional triaxial test is given by:

$$\Delta V/V_{\text{elastic}} = \frac{1-2\nu}{E}(\sigma_1 - \sigma_3) \tag{3}$$

where E is Young's modulus and ν is Poisson's ratio. This strain component can be calculated assuming linear elasticity, if the mechanical constants of the material are known.

The analytical expression for crack initiation stress is dependent upon the length of the initial flaw $2a$. It is commonly assumed that the initial flaw is scaled by the mean grain size in polycrystalline rocks [4, 5]. However, in carbonate rocks in general and particularly in dolomites, grain arrangement can vary between samples, as well as grain size. Textural variations have a distinct influence on fracture propagation mode and consequently on rock strength. Hatzor *et al.* [11] for example, have defined two propagation modes in dolomites based on mechanical tests, petrographic analysis and SEM observations.

We first present the results of a series of uniaxial and triaxial compression tests performed on several dolomite samples of varying porosity and mean grain size. We check the validity of the Ashby and Hallam expression [equation (2)], assuming that initial flaws are scaled by mean grain size. We then proceed and propose an empirical model which predicts crack initiation stress as a composite function of porosity, and mean grain size. Finally, we develop a new model, based on Griffith crack theory and our empirical model, which predicts the size of the initial flaw, in terms of porosity and mean grain size.

EXPERIMENTAL PROCEDURES

The tested material

In this study 32 samples of dolomites were tested. The tested dolomites belong to the Aminadav Formation, an Upper Cretaceous dolomite formation of wide distribution in central Israel. The samples were retrieved from depths of up to 300 m. The rock typically contains 100% dolomite, having relatively low porosity ranging between 2 and 21%. The rock specimens are typically isotropic but inhomogeneous, a single specimen may contain a range of grain sizes in different types of arrangements (Fig. 1). The grain size values span two orders of magnitude, from several micrometers up to 200 micrometers (Table 1).

In order to determine the porosity (n) of the specimens a solid sample from each was ground and the specific weight of solids (G_s) was measured according to ASTM standards. Right circular cylinders were prepared following ISRM standards with a diameter of 54 mm and an L to D ratio of 2.0 or slightly above. Specimen ends were ground to a flatness of 0.02 mm in order to minimize end effects. The initial volume of each specimen was measured using a digital caliper with resolution of 0.01 mm and the dry mass was measured using a digital scale with a resolution of 0.01 g, so that dry bulk density was determined with an accuracy of 0.01 g/cm^3. The precision of the porosity estimation is believed to be within 0.01%.

Petrographic analysis

Each tested sample was studied using a petrographic microscope and scanning electron microscope (SEM). Thin sections were prepared from the specimen material before loading in order to define the grain size distribution and arrangement. SEM analysis was performed on material which was sampled from the failure zone in each specimen after loading, in order to study the details of the texture and grain size distribution, and in order to identify the fracture initiation and propagation mechanisms.

Testing procedures

Mechanical testing was performed using a stiff load frame (5×10^9 N/m) operated hydraulically by closed loop servo control (TerraTek model FX-S-33090), with a maximum axial load capacity of 1.4 MN and confining pressure capacity of 70 MPa. Control was achieved by axial displacement monitoring and tests were run at a constant strain rate of 1×10^{-5} l/sec. Piston displacement was monitored using a high sensitivity LVDT located outside the vessel. Load was measured by a sensitive load cell located in series with the sample stack, having a maximum capacity of 1000 kN and linearity of 0.5% full scale.

In only 17 out of the 32 tests was complete monitoring of axial and radial strains performed using a strain monitoring system attached to the sample. Axial and radial strains were recorded using four arm axial and transverse strain cantilever sets. Using the cantilever sets, three independent strain axes in parallel with the three principal stress axes were monitored, and thus volumetric strain calculations were enabled by summation of the three orthogonal normal strains: $\varepsilon_v = \varepsilon_a + \varepsilon_{r1} + \varepsilon_{r2} = \varepsilon_1 + \varepsilon_2 + \varepsilon_3$ where ε_v is the volumetric strain, ε_a is the axial strain, ε_{ri} is a transverse strain and ε_i is a principal strain. Only the results of the 17 fully monitored tests are shown here. The results of the entire testing program are published elsewhere [11].

EXPERIMENTAL RESULTS

Physical properties

The physical properties of the tested samples are summarized in Table 1. Calculated porosity values vary

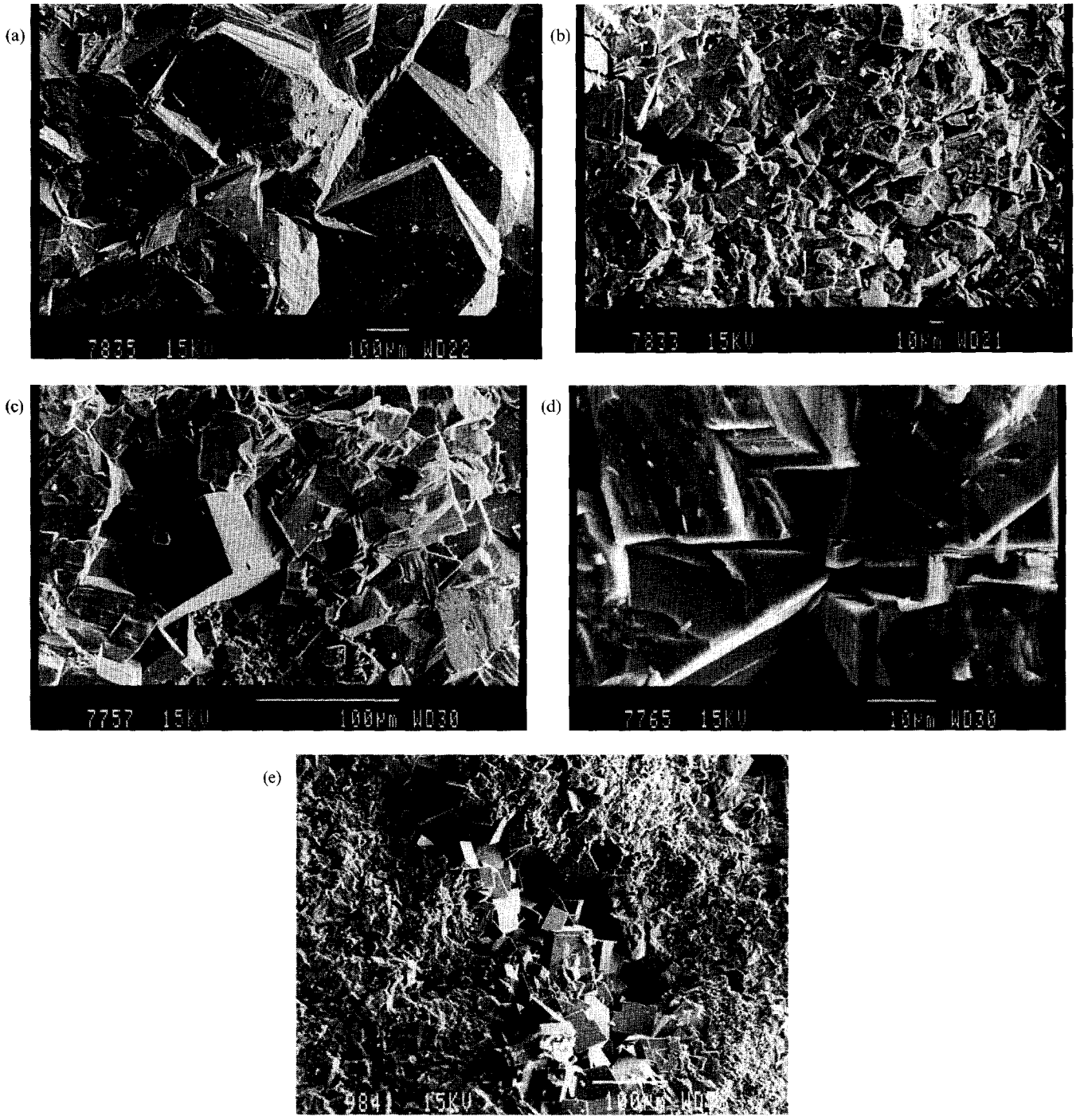

Fig. 1. Three different mosaic textures in the studied dolomites. (a) Xenotopic mosaic texture with planar face to face contacts between crystals (SEM picture 7835); (b) Intercrystalline crack propagation mechanism (SEM picture 7833) in xenotopic texture; (c) Hypidiotopic mosaic texture with angular edge to face contacts (SEM picture 7757); (d) Intracrystalline crack propagation mechanism (SEM picture 7765) in hypidiotopic mosaic; and (e) Idiotopic mosaic texture with completely developed crystal faces filling available void space (SEM picture 9841).

Table 1. Physical properties of studied dolomites

Sample	Density ρ (g/cm^3)	Porosity n (%)	Grain size using SEM (μm) Mean	Mode	Max
AD-2	2.75	2	49	45	88
AD-5	2.62	5.8	35	24	63
AD-13	2.68	3.6	25	32	40
AD-15	2.19	20.9	33	35	71
AD-18	2.58	7.9	17	18	33
AD-31	2.66	4.6	50	62	127
AD-34	2.68	4.24	21	21	46
AD-37	2.41	13.8	9	6	108
AD-43	2.65	5.4	24	20	154
AD-80	2.62	6.4	26.9	15	69.2
AD-81	2.61	6.8	27.5	18.3	73
AD-81A	2.64	5.7	27.5	18.3	73
AD-82	2.52	10	19.2	13.3	84.6
AD-82A	2.43	13.2	19.2	13.3	84.6
AD-83	2.37	15.4	27.3	16.6	70
AD-8A	2.3	17.9	27.3	16.6	70
AD-84	2.64	5.7	33.2	11.4	103.5

between 2 and 21% with an average value of 7.5%. The modes of the grain size distribution in each sample are given using the higher accuracy SEM results. The grain size distributions are typically unimodal and asymmetric with greater frequency of the smaller sizes. Mean grain size values detected using SEM are between 9 and 50 micrometers and maximum values are 33–154 micrometers. Typically, a larger span of size distributions was detected using the petrographic microscope.

Petrographic analysis

Three mosaic textures were found in the studied dolomites. In Fig. 1, Scanning Electron Microscope (SEM) photographs of the typical mosaic textures are shown. In the "xenotopic" mosaic texture [Fig. 1(a)] closely packed anhedral crystals with irregular intercrystalline boundaries are common. In the "hypidiotopic" mosaic texture [Fig. 1(c)] most dolomite crystals are subhedral to anhedral with straight compromise boundaries and common crystal–face junctions. The "idiotopic" mosaic texture [Fig. 1(e)] is characterized by euhedral dolomite crystals exhibiting rhombohedral geometry (petrographic description of the three textures after Tucker and Wright [12]). The three mosaic textures may co-exist, in varying proportions, in a single specimen, however, typically each specimen can be characterized with a single predominant texture. The dominant mosaic texture in each sample is listed in Table 2.

Hatzor *et al.* [11] have defined two propagation modes in dolomites based on mechanical tests, petrographic analysis and SEM observations: (1) Intercrystalline fracture, commonly observed in xenotopic mosaic textures, in which fracture is enabled by separation of face to face contacts [Fig. 1(a) and (b)], and (2) Intracrystalline propagation mode, typically observed in hypidiotopic mosaic textures, in which propagation induces fracture of intact crystals, due to the abundance of face to edge contacts [Fig. 1(c) and (d)]. These different propagation mechanisms lead to differences in strength. In a specimen containing hypidiotopic mosaic, where post failure intracrystalline fractures were detected, peak stress at unconfined compression was found to be 2.8 times higher than in a specimen containing the xenotopic mosaic texture, in which intercrystalline fractures were observed after failure (274 MPa and 98 MPa in samples AD43 and AD5, respectively, Table 2). The crack initiation stress (defined in the following section) in the hypidiotopic mosaic texture was 1.91 times higher than in the xenotopic mosaic texture (165 MPa and 83 MPa, respectively). The mean grain sizes were 24 μm and 35 μm in the stronger and weaker specimens, respectively (Table 1). This difference in mean grain size would result in a crack initiation stress increase of 1.2 times only, according to the analytical expression in equation (2), much less than is actually observed. The difference between observations and predictions is explained here by the influence of rock texture.

The quantification of grain arrangement, or texture, is not simple because one or two mosaic textures may

Table 2. Mechanical test results of studied dolomites

Sample	P_c (MPa)	E (GPa)	ν	ε_i	σ_i (MPa)	σ_d (MPa)	σ_p (MPa)	Type of dominant mosaic texture
AD-2	0	70	0.16	0.00095	85	102	117	xenotopic
AD-5	0	56	0.37	0.0006	83	85	98	xenotopic
AD-13	10	61	0.25	0.0021	238	243	243	hypidiotopic
AD-15	0	29	0.26	0.0008	39	57	67	idiotopic
AD-18	7	58	0.30	0.0009	126	158	202	idiotopic
AD-31	10	42	0.3	0.00149	100	174	191	idiotopic
AD-34	25	63.8	0.28	0.00125	205	290	315	idiotopic
AD-37	15	28	0.35	0.0012	130	138	142	xenotopic
AD-43	0	64	0.27	0.0018	165	274	274	hypidiotopic
AD-80	0	58.5	0.28	0.0008	102	174	174	hypidiotopic
AD-81	5	59.2	0.18	0.0008	90	110	154	idiotopic
AD-81A	10	57	0.27	0.0013	135	230	255	idiotopic
AD-82	10	43	0.22	0.0013	110	162	173	hypidiotopic
AD-82A	15	41	0.25	0.0013	90	186	210	hypidiotopic
AD-83	0	18	0.25	0.0007	43	43	62	xenotopic
AD-83A	5	19.6	0.24	0.0013	45	52	70	xenotopic
AD-84	10	49.3	0.26	0.001	100	120	166	hypidiotopic

P_c = confining pressure; E = Young's modulus; ν = Poission's ratio; ε_i = volumetric strain at crack initiation; σ_i = stress difference at crack initiation; σ_d = stress difference at onset of dilation; σ_p = peak stress difference.

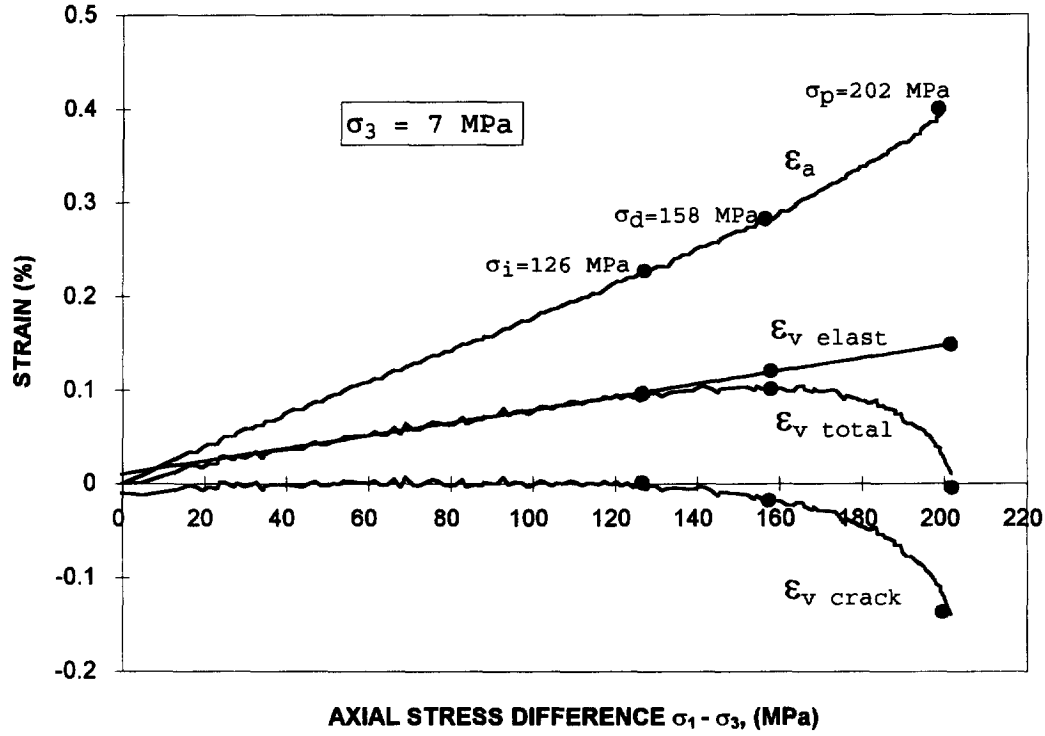

Fig. 2. Definition of crack initiation stress (σ_i = 126 MPa), onset of unstable cracking (σ_d = 158 MPa), and ultimate strength (σ_p = 202 MPa) using data from specimen AD18 tested under a 7 MPa confining pressure [10]. ε_a = axial strain, $\varepsilon v_{elast.}$ = elastic volumetric strain, εv_{total} = total volumetric strain and εv_{crack} = crack volumetric strain.

co-exist within a single specimen in varying proportions. In this paper we use porosity as a quantitative measure of texture in order to test the influence of texture on crack initiation stress. Porosity is a measurable index property and is a manifestation of grain arrangement. Closely packed mosaic textures like hypidiotopic are expected to exhibit low porosity, whereas idiotopic mosaic textures [Fig. 1(e)] in which voids and cement inhibit the intergranular space, represent the higher porosity samples. The porosity in xenotopic mosaic textures lies within these two extremes.

Mechanical test results

The mechanical parameter which is of prime interest in this study is the crack initiation stress, the attainment of which indicates the onset of inelastic deformation. The inelastic volumetric strain component in triaxial compression is attributed to the opening of micro-cracks during application of deviator stress, a process defined by Brace *et al.* [13] as dilatancy. The inelastic volumetric strain or crack volumetric strain [10] is given by the difference between the total and elastic volumetric strain components, as shown in Fig. 2, using data from sample

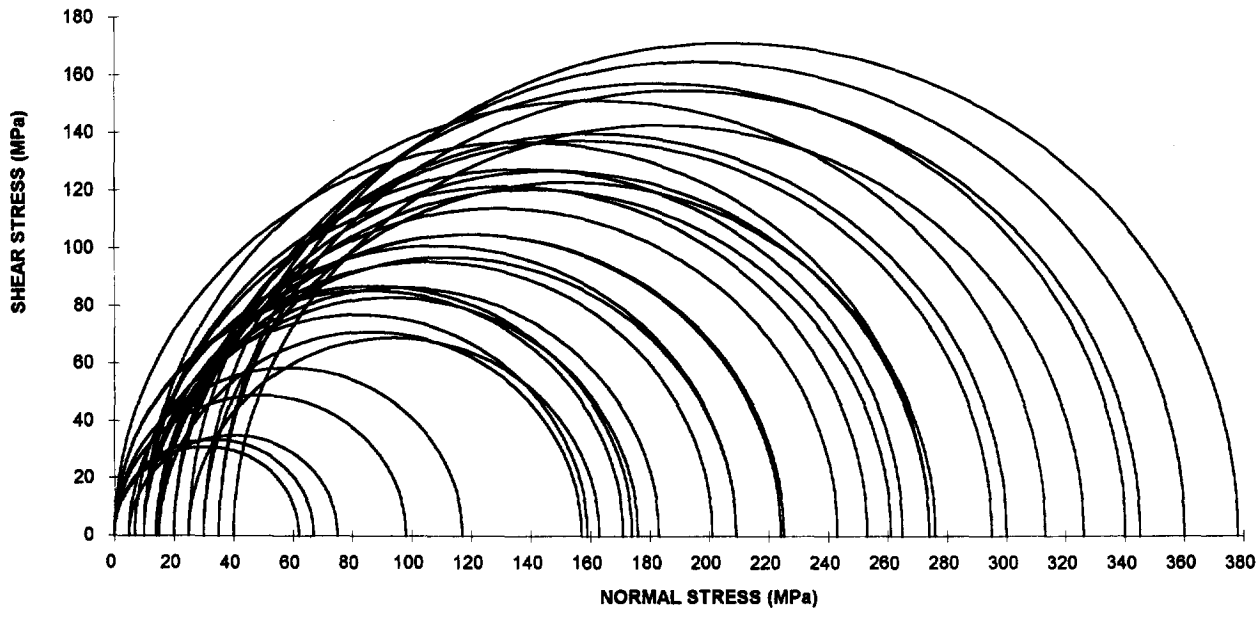

Fig. 3. Mohr circles for peak principal stresses (at failure) for the studied dolomites of Aminadav formation, Israel.

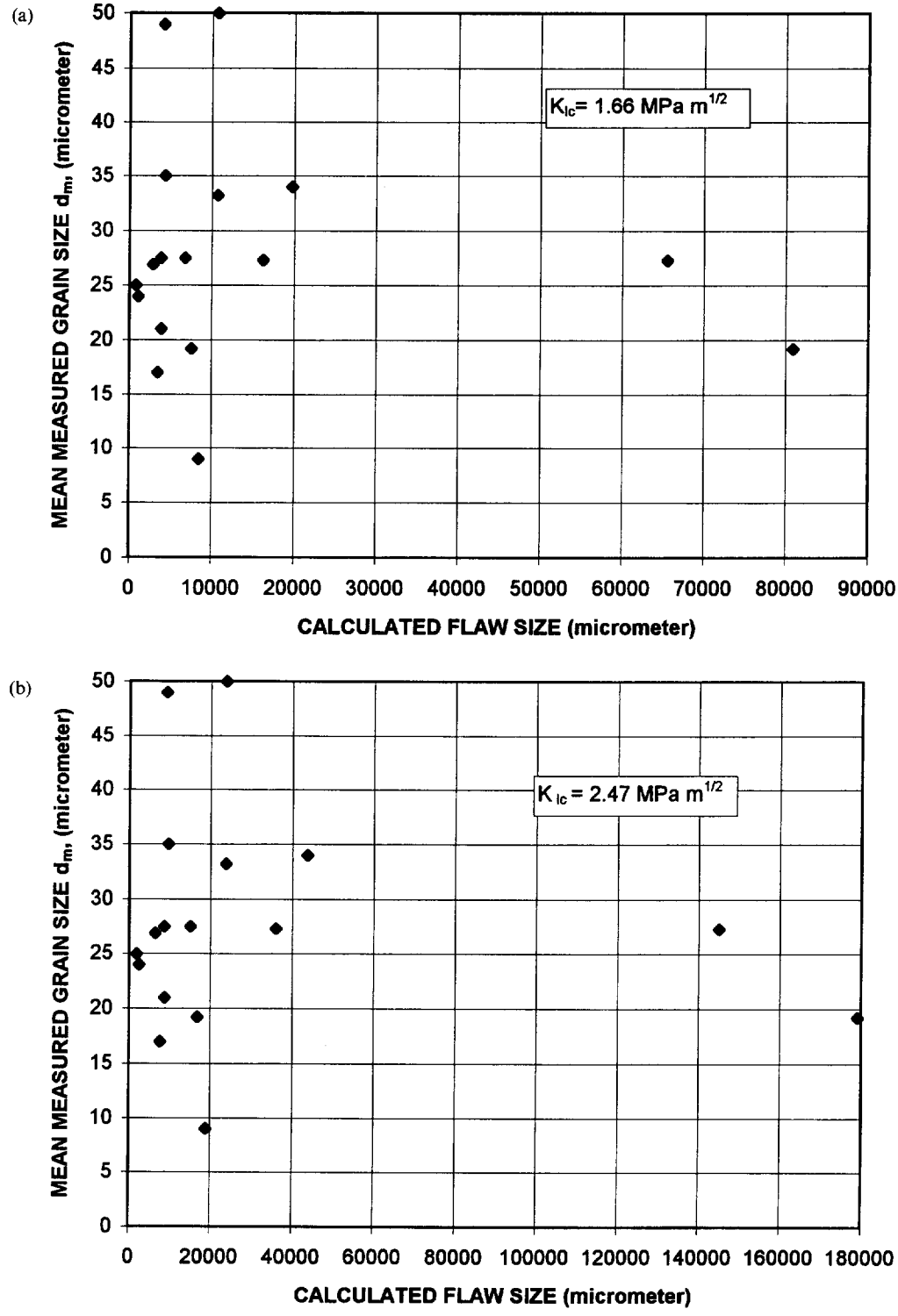

Fig. 4. Comparison between calculated critical flaw size [equation (2)] and measured mean grain size (micrometers) in tested samples. (a) K_{Ic} = 1.66 MPa $m^{1/2}$, (b) K_{Ic} = 2.47 MPa $m^{1/2}$.

AD-18 of this study (Table 2). With application of axial stress difference, crack closure is responsible for the noted decrease in crack volumetric strain. During elastic loading the crack volumetric strain should be zero, as no inelastic deformation takes place. Crack initiation is marked by an increase in crack volumetric strain. The stress difference at that stage is defined as the crack initiation stress (σ_i), given by the difference between σ_1 and σ_3. Unstable cracking is attributed to the deflection point in the total volumetric strain curve [14]. This point has been originally defined by Brace *et al.* [13] as onset of dilatancy.

The results of the fully monitored mechanical tests are summarized in Table 2. The Young's modulus values range between 18 and 70 GPa, and Poisson's ratio varies between 0.16 and 0.37. Ultimate strength values (σ_p) in a given confining pressure level vary considerably. E.g. in unconfined compression ultimate strength varies between 62 and 274 MPa in samples AD83 and AD43, respectively (Table 2). The strength increase

Table 3. Empirical coefficient values found for tested dolomites in this study

Parameter	A	B	C	D (MPa mm)
Value	0.025	680	0.92	1

Parameters A, B and C are dimensionless, the units of parameter D are MPa mm.

cannot be attributed to mean grain size alone, as the mean grain size values are similar (Table 1). The porosity values, however, are very different, the weaker sample having a porosity of 15% and the stronger sample having a porosity of 5.4%. Crack initiation (σ_i) is detected at 52–98% ultimate strength, with an average value of 72%. Unstable cracking is detected at *ca.* 90% ultimate strength. The influence of grain size and porosity on crack initiation stress is explored in the following sections.

CRACK INITIATION STRESS—ANALYTICAL APPROACH

The analytical expression for a Mode I critical stress intensity factor at crack initiation, according to the sliding crack model, predicts a linear relation between the principal compressive stress at initiation (σ_{1i}) and the inverse square root of half the flaw size $a^{-1/2}$ [equation (2)]. It is commonly assumed that mean grain size in crystalline rocks is a good measure of the initial flaw size [4, 5]. In order to test this hypothesis the critical flaw size at crack initiation was calculated using equation (2), for the level of principal compressive stress at crack initiation ($\sigma_i + P_c$). In order to perform this calculation the value of the stress intensity resistance (K_{Ic}) for the studied dolomites is required, as well as the value of the coefficient of internal friction (μ). In Fig. 3 principal stress values at failure are plotted in a Mohr diagram space (shear stress vs normal stress) for all the 32 tested dolomites. Linear regression performed in principal stress space ($\sigma_{1,p}$ vs σ_3), assuming a Coulomb–Mohr failure envelope, yielded the following mechanical parameters for Aminadav dolomite: cohesion = 30 MPa; unconfined compressive strength = 143.5 MPa; and internal friction angle = 44.6°. Considering these material properties of Aminadav formation an average value of $\mu = 0.98$ was used in the analysis. Experimental values for K_{Ic} for the studied dolomites are not available at the present time. A range of values for dolomites is quoted by Atkinson and Meredith [15]. A relatively low value of 1.66 MPa $m^{1/2}$ for Kankakee dolstone, and a relatively high value of 2.47 MPa $m^{1/2}$ for Romeo dolstone were reported by Gunsallus and Kulhawy [16]. These two extreme values were used in the analysis here. The comparison between the calculated and observed values is shown in Fig. 4(a) and (b) using the K_{Ic} values of 1.66 and 2.47 MPa $m^{1/2}$, respectively. It can be clearly seen that a great discrepancy exists. While the observed mean grain size is between 10 and 50 μm, the calculated initial flaw size is two–three orders of magnitude higher in both cases. This discrepancy cannot be explained in terms of grain size statistics, because even the maximum grain size, detected by petrographic microscope observations, never exceeds 1000 μm.

The result of this analysis suggests that other, more complex initiation processes take place, which are necessarily influenced by grain arrangement or rock texture in general. While an attempt has been made to

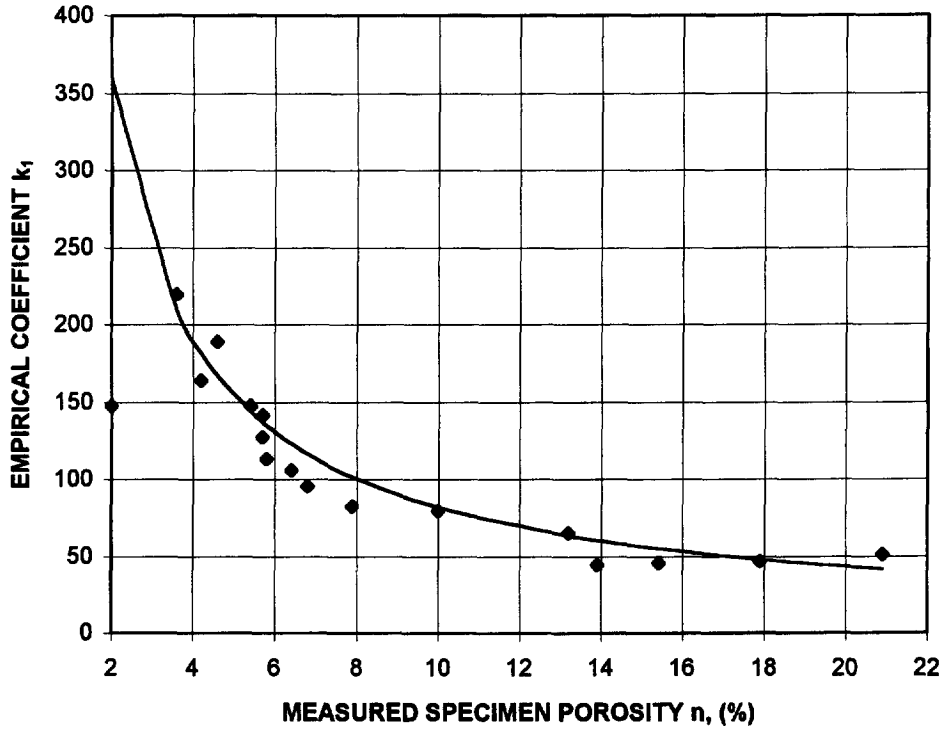

Fig. 5. Predictive capability of empirical coefficient k_1 from application of equation (4) using data from tested samples. The model loses validity for porosity values smaller than 2%.

describe two plausible modes of fracture propagation in various dolomite textures [11], a modification of the analytical expression for stress intensity [equation (2)] is not proposed here. Instead, the relation between the dominant parameters is defined empirically, using the statistical model developed below.

CRACK INITIATION STRESS—EMPIRICAL MODEL

Quantification of rock texture is possible if we use the porosity values that were accurately estimated for each sample. The underlying assumption here is that porosity scales texture but is independent of grain size. We wish to find how both porosity and grain size influence crack initiation stress, and for that we use three measurable quantities: ε_i—total volumetric strain at crack initiation; n (%)—estimated porosity; and d_m (mm)—mean grain size. The data used for the analysis are listed in Tables 1 and 2. These data are approximated by the following empirical model:

$$\sigma_i = k_1 k_2 (\varepsilon_i + A) \tag{4}$$

where σ_i is the stress difference $(\sigma_1 - \sigma_3)$ at crack initiation; $k_1 = B/n^C$; and $k_2 = D/d_m$. A, B, C and D are empirical parameters, the values of which are listed in Table 3. The applicability of the model for the entire test data set is shown in Fig. 5, where measured values of porosity (Table 1), crack initiation stress and total volumetric strain at crack initiation (Table 2), were inserted into equation (4) in order to evaluate k_1. It can be clearly seen that the empirical coefficient k_1 is inapplicable for porosity values lower than 2%. For porosity values greater than 2% the model is expected to be valid.

The applicability of the model for porosity values greater than 2% is shown in Fig. 6, in which the calculated flaw size of crack initiation by equation (4) is compared with the measured value of the mean grain size by SEM in each sample. The calculated value of flaw size at crack initiation is given by:

$$d_m = \frac{B(\varepsilon_i + A)}{\sigma_i n^C}. \tag{5}$$

The linear regression coefficient that is obtained in Fig. 6 is 0.83.

Equation (4) can be further developed using the theory of elasticity. The total volumetric strain at crack initiation is given by:

$$\varepsilon_i = \frac{(1 - 2\nu)\,\sigma_i}{E} \tag{6}$$

where E and ν are Young's modulus and Poisson's ratio, respectively. Inserting equation (6) into equation (4), the final model for stress difference at crack initiation stress is obtained:

$$\sigma_i = \frac{A}{\left(\frac{d_m n^C}{BD}\right) - \left(\frac{1 - 2\nu}{E}\right)}. \tag{7}$$

The final model indicates that crack initiation stress is inversely proportional to both mean grain size and porosity. A two dimensional presentation of equation (7) is shown in Fig. 7 for four different porosity values, assuming an average value of 9.82×10^{-6} MPa^{-1} for the elasticity expression: $(1 - 2\nu)/E$, using the data for all tests (Table 2). The surface which is obtained from the relationship between σ_i, n and d_m is shown in Fig. 8 in which x is porosity, y is mean grain size, and z is stress difference at crack initiation.

From Figs 7 and 8 the following conclusions emerge:

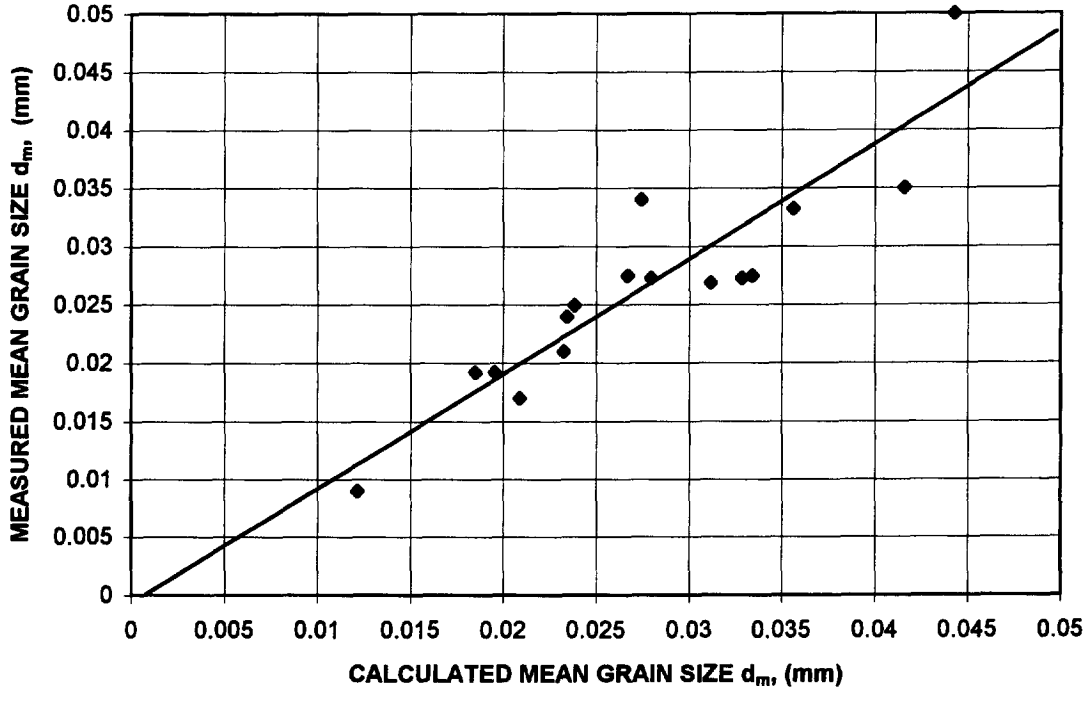

Fig. 6. Correlation between calculated mean grain size using statistical model [equation (5)] and actual SEM observations.

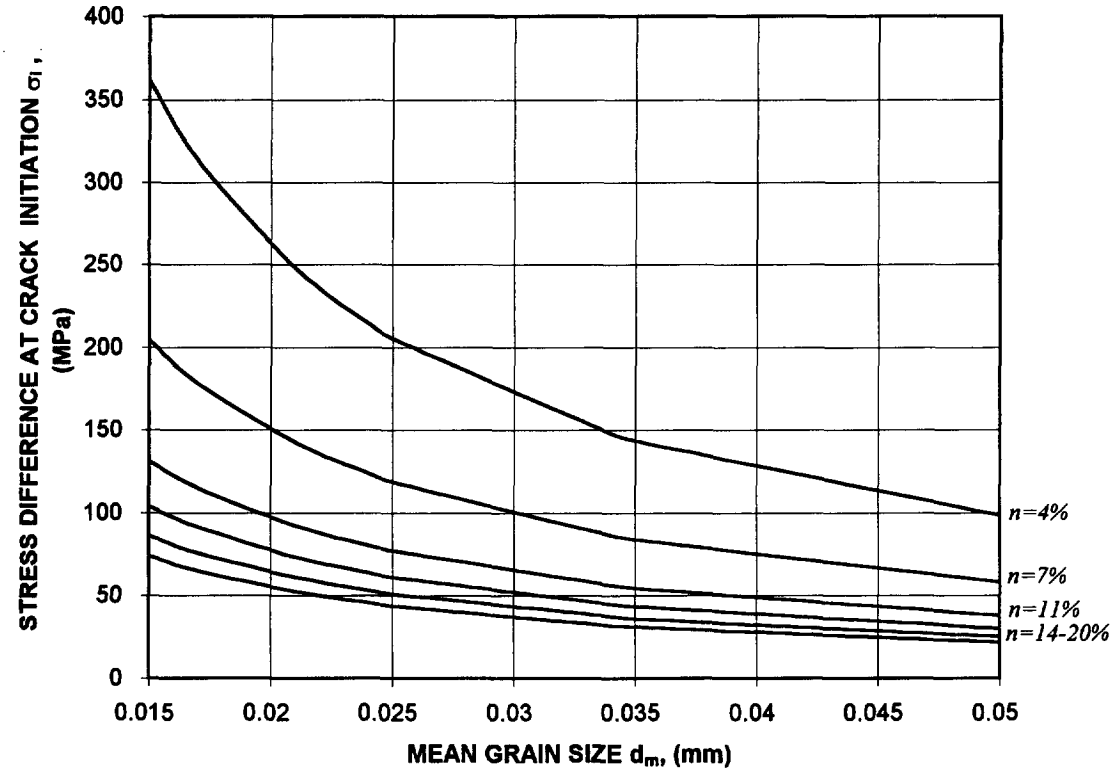

Fig. 7. Relationship between crack initiation stress and mean grain size for different values of porosity according to the statistical model [equation (7)].

(1) The crack initiation stress surface slopes concavely downwards from low porosity–low grain size to high porosity–high grain size. (2) When porosity is low the sensitivity of σ_i to mean grain size is very high. This effect is reduced with higher porosity values. (3) When grain size is small the influence of porosity on σ_i is very pronounced; this effect is reduced as grain size is increased.

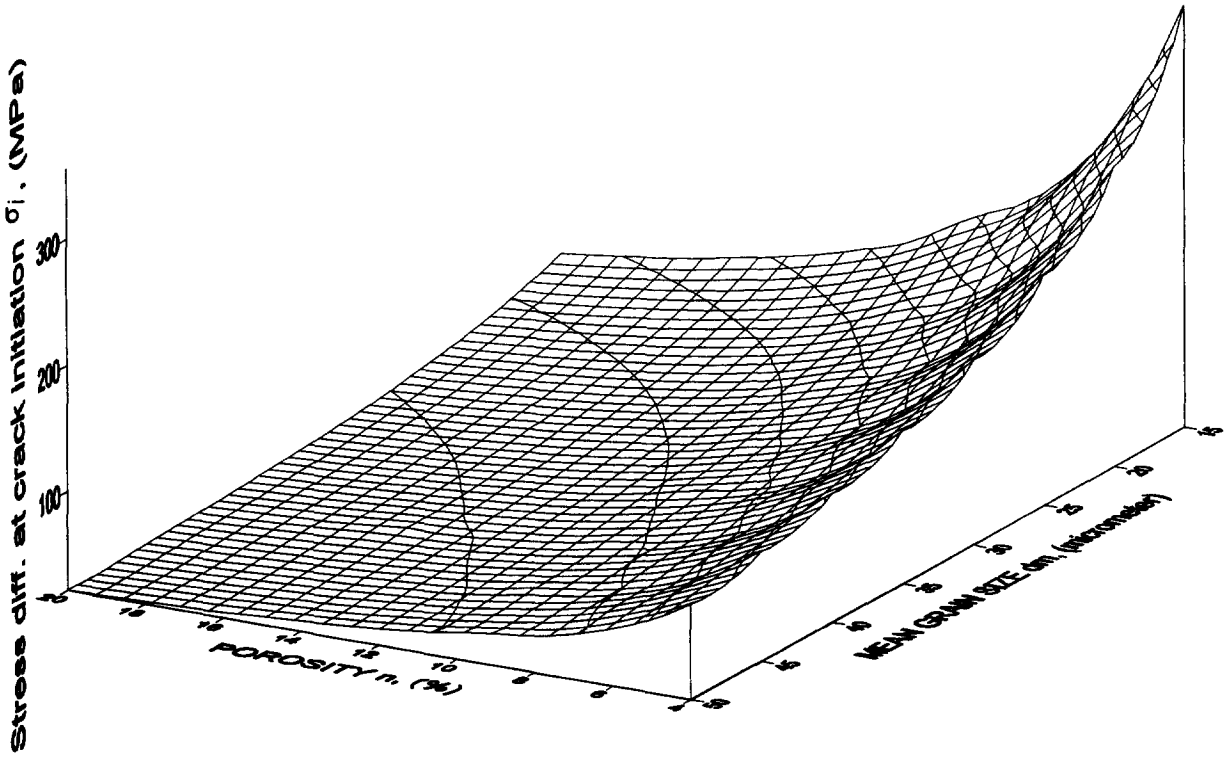

Fig. 8. Three dimensional representation of the relationship between mean grain size, porosity and crack initiation stress, scaled for studied dolomites [equation (7)].

Table 4. Relationship between mean grain size and calculated initial flaw size in the tested samples

Sample	d_m (mm)	L_i (mm)	L_i/d_m	n (%)
AD-2	0.035	0.134	3.84	5.8
AD-13	0.025	0.028	1.12	3.6
AD-15	0.034	0.69	20.3	20.9
AD-18	0.017	0.055	3.25	7.9
AD-31	0.05	0.13	2.61	4.6
AD-34	0.021	0.028	1.33	4.24
AD-37	0.009	0.02	2.2	13.8
AD-43	0.024	0.06	2.5	5.4
AD-80	0.0269	0.096	3.57	6.4
AD-81	0.0275	0.11	4.03	6.8
AD-81A	0.0275	0.078	2.84	5.7
AD-82	0.0192	0.078	4.07	10
AD-82A	0.0192	0.128	6.69	13.2
AD-83	0.0273	0.146	5.36	15.4
AD-83A	0.0273	0.21	7.85	17.9
AD-84	0.0332	0.098	2.69	5.7

d_m = mean grain size; L_i = initial flaw length; n = porosity.

DISCUSSION

Griffith [17] assumed that stress concentrations at the tip of minute cracks lead to macroscopic failure of brittle materials. It has been common to assume in rock mechanics that grain boundaries can function as potential Griffith cracks. It has been shown above that there are two textural parameters which must be considered, however, grain size and porosity. In this section we will try to incorporate these parameters and our empirical model, into the classical criteria of Griffith.

According to Griffith, mode I fracture is initiated when the applied remote stress attains a critical value (σ_i) which depends upon the length of the initial crack $2a$ (where a is the half length of the initial crack), the specific surface energy per unit length of crack surface (γ), and the modulus of elasticity of the rock:

$$\sigma_i = \sqrt{\frac{2E\gamma}{\pi a}}. \tag{8}$$

The half length of the critical initial crack is therefore

$$a = \frac{2E\gamma}{\pi\sigma_i^2} \tag{9}$$

and the initial crack length according to the Griffith model is

$$L_i = 2a = \frac{1.273\gamma E}{\sigma_i^2}. \tag{10}$$

We can now express σ_i in terms of mean grain size, porosity, total volumetric strain at crack initiation stress and the elastic constants to obtain the critical flaw length L_i, where L_i is the length of the initial flaw in mm; γ is the specific energy in MPa mm; E is the elastic modulus in MPa; and d_m is the mean grain size in mm:

$$L_i = 1.273\gamma E \frac{\left[\frac{d_m n^C}{BD} - \frac{1-2\nu}{E}\right]^2}{A^2}. \tag{11}$$

The new expression for initial flaw length [equation (11)] predicts that L_i increases with increasing mean grain size, porosity and elastic modulus. This prediction is intuitively appealing. Consider sandstone and claystone, for example. In sandstone the elastic modulus, the mean grain size and the porosity are typically much higher than in claystone. Indeed the size of the initial flaws in claystone is several orders of magnitude smaller

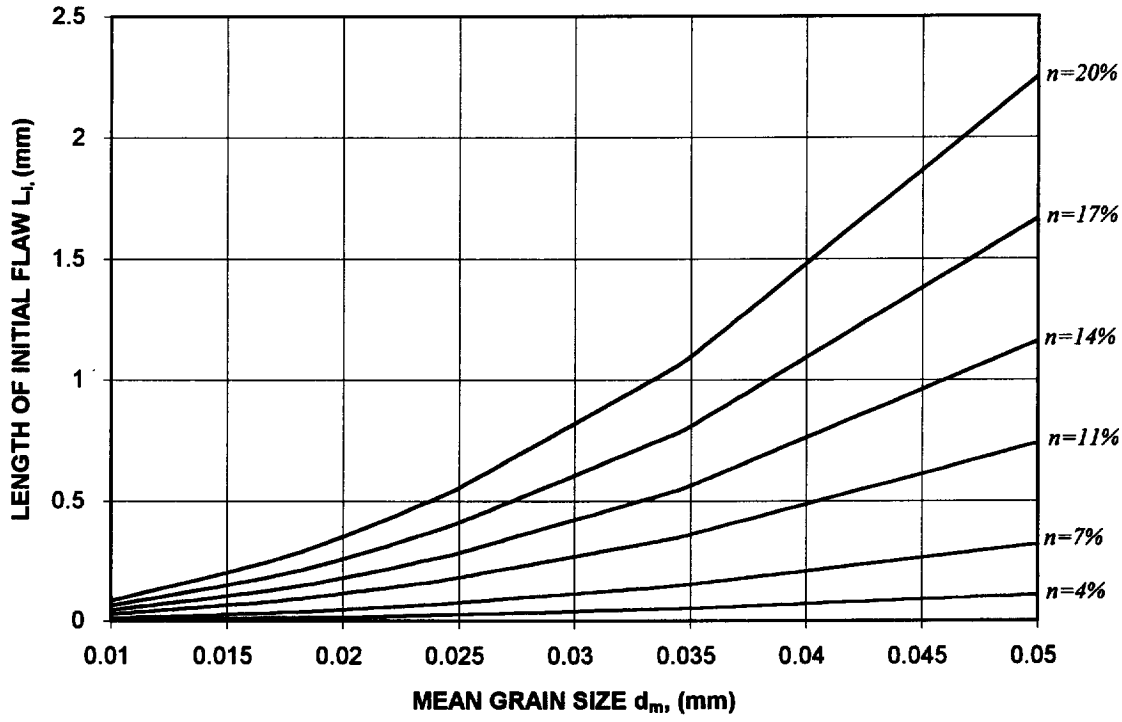

Fig. 9. Relationship between Griffith crack length and mean grain size for different porosity values in studied dolomites according to the suggested model [equation (11)].

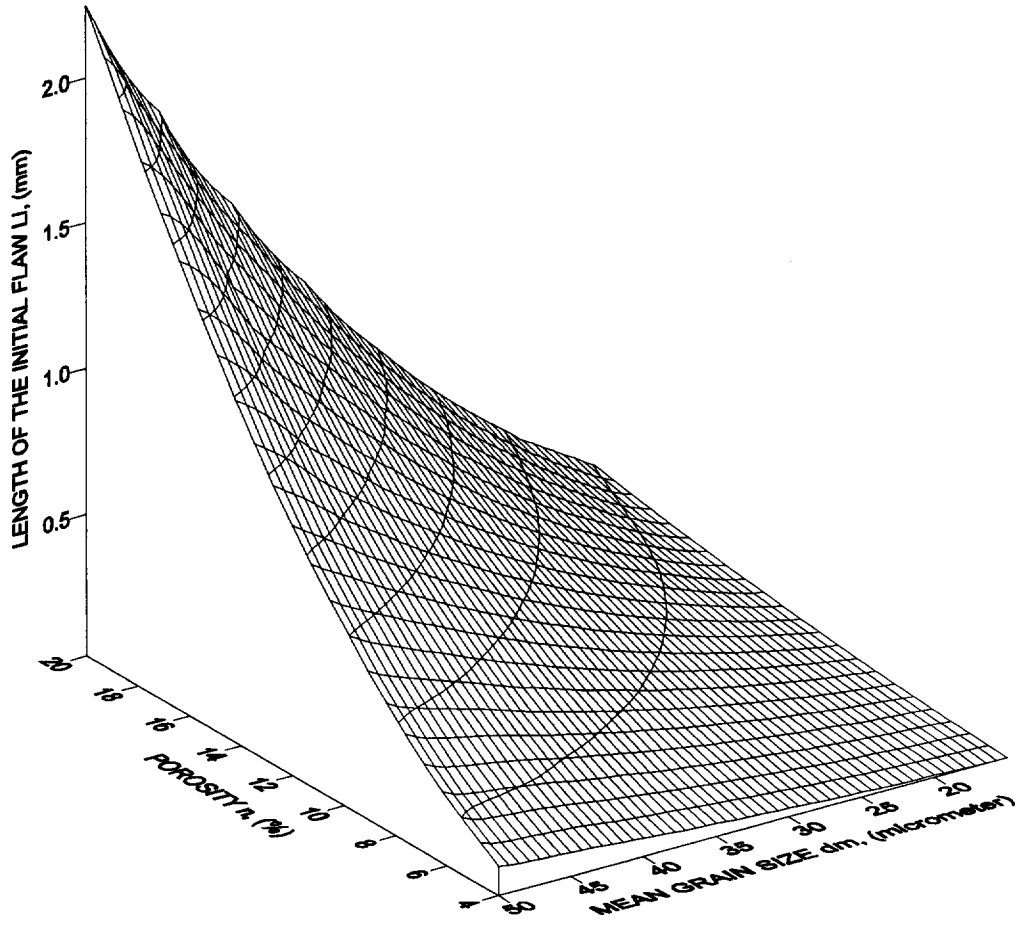

Fig. 10. Three dimensional representation of the relationship between the mean grain size, porosity and the length of the critical flaw size, scaled for the studied dolomites.

than in sandstone, assuming that in claystone the clay mineral faces function as initial flaws.

Assuming, e.g. that the surface energy per unit length of crack surface is 0.018 MPa mm, as found for concrete and rocks at crack initiation by Kaplan [18], we can calculate the ratio between measured mean grain size and calculated initial flaw size for our tested samples, using equation (11). This ratio is shown in Table 4. At low porosity values (near 4%) the ratio is *ca.* 1.0, i.e. in a closely packed mosaic texture, the initial flaw is very likely to be a single grain boundary. However, at a porosity value of 21% (sample AD15), the initial flaw length is 20 times higher than the mean grain size.

The mathematical relation between L_i and mean grain size is plotted in Fig. 9 for six porosity values, assuming a surface energy value of $\gamma = 0.018$ MPa mm, and a Young's modulus value of 46.7 GPa. The three-dimensional surface of L_i (Fig. 10) is sloping concavely downward from high porosity–high grain size ($n = 20\%$, $d_m = 50\ \mu m$) to low porosity—low grain size ($n = 4\%$, $d_m = 10\ \mu m$). When porosity and mean grain size decreases simultaneously, the initial flaw length is reduced by two orders of magnitude (from 2.2 mm to 0.01 mm), and approaches the mean grain size value ($d_m = 0.01$ mm, $n = 4\%$, $L_i = 0.01$ mm).

When porosity is kept constant and mean grain size is increased, the proportional increase in initial flaw length is approximately the same for all porosity values—about one order of magnitude. This is also true in the opposite case when mean grain size is kept constant and porosity is increased. The proportional increase in initial flaw length is *ca.* one order of magnitude for all mean grain size values. When porosity is increased and mean grain size is decreased, there is no net effect on the initial flaw length, as can be inferred from Fig. 10 when traveling along the diagonal which connects the coordinates (low d_m, high n) and (high d_m, low n).

The assumption of the sliding crack mechanism in polycrystalline aggregates leads to the expectation that crack initiation and ultimate stresses are linearly related to the inverse square root of the mean grain size [1, 4, 5] since existing grain boundaries are assumed to function as initial flaws, and therefore as stress concentrators [3]. The longer the initial crack, the higher the stress concentration (K_L) and therefore the lower the remote stress level (σ_1) required for fracture initiation, and consequently for attainment of ultimate stress.

It may be concluded from this discussion that the above assumption regarding initial flaw size as equal to mean grain size is valid only in the very restricted case of low porosity–low grain size rocks. In such rock textures the void space is minimal and available crystal faces may function as truly initial flaws, provided that

fracture propagation from the edge of the flaws is possible. In such low porosity textures, variations in mean grain size influence crack initiation stress significantly (Fig. 8), indicating that in low porosity textures the role of individual grains as stress concentrators is significant. In porous rocks, however, the initial flaw length may be up to two orders of magnitude higher than the mean grain size in the rock, depending upon the porosity and mean grain size. The initial crack in such textures must therefore be the union of several crystal faces, properly aligned with respect to the maximum principal compressive stress direction. Indeed in high porosity rocks, crack initiation stress is much less sensitive to variations in mean grain size (Fig. 8), indicating that the role of individual grains is less significant.

SUMMARY AND CONCLUSIONS

In order to quantify the influence of rock texture on fracture initiation stress, porosity and grain size are used under the assumption that porosity scales texture, and is independent of grain size. It is demonstrated empirically that fracture initiation stress is inversely related to both mean grain size and porosity for monomineralic dolomite. The three-dimensional relation is represented by a surface of fracture initiation stress which concavely declines from low porosity–low grain size to high porosity–high grain size coordinate. The influence of grain size on crack initiation stress is more pronounced in low porosity than in higher porosity rocks. The influence of porosity on crack initiation stress is more pronounced in low grain size rocks.

Based on experimental data, the developed empirical model for fracture initiation stress and Griffith fracture initiation criteria, a model for initial flaw length is proposed. The model predicts that initial flaw length is directly proportional to the elastic modulus, mean grain size and the porosity. The predicted surface concavely declines from high porosity–high mean grain size, to a low porosity–low mean grain size coordinate. It is shown that only at the extreme case of low porosity–low mean grain size, the initial flaw length approaches the mean grain size length in the sample. Hence, the conventional rock mechanics assumption that grain size is a suitable scale for initial flaw length, is in fact erroneous in the general case and is only correct in the restricted case of small porosity–small grain size textural arrangements.

In low porosity rocks, crack initiation stress is extremely sensitive to mean grain size and initial flaw length is shown to approach the mean grain size value. These findings confirm that in low porosity textures the effect of individual grains on fracture initiation stress is very significant, probably because individual grain boundaries function as true initial flaws. In higher porosity textures, crack initiation stress is much less sensitive to mean grain size and initial flaw length is shown to be higher by up to two orders of magnitudes than the mean grain size value. These findings suggest that the effect of individual grain boundaries in high porosity textures is less significant, rather, the union of several individual grain boundaries may function as the initial stress concentrator.

Acknowledgements—This research was supported by a grant from the Earth Science Administration, the Ministry of Energy and Infrastructure, State of Israel, through contracts No. 93-17-022 and 94-17-041. Y. Mimran of the Geological Survey of Israel has provided helpful advice with SEM observations and his assistance is acknowledged. A. Zur of Ben-Gurion University has measured grain size distribution in all samples and his careful work is greatly acknowledged.

Accepted for publication 29 November 1996.

REFERENCES

1. Hugman, R. H. H. and Friedman, M., Effects of texture and composition on mechanical behavior of experimentally deformed carbonate rocks. *Am. Assoc. Pet. Geol. Bull.*, 1979, **63**, 1478–1489.
2. Olsson, W. A., Grain size dependence of yield stress in marble. *J. Geophys. Res.*, 1974, **79**, 4859–4862.
3. Petch, N. J., The cleavage strength of polycrystals. *J. Iron Steel Inst.*, 1953, 25–28.
4. Fredrich, J. T., Evans, B. and Wong, T. F., Effects of grain size on brittle and semibrittle strength: implications for micromechanical modelling of failure in compression. *J. Geophys. Res.*, 1990, **95**, 10,907–10,920.
5. Wong, H. C., Chau, K. T. and Wang, P., Microcracking in coarse and fine grain marbles. In *Proc. 35th U.S. Symp. on Rock Mechanics, Lake Tahoe*, eds J. J. K. Daemen and R. A. Schultz. Balkema, Rotterdam, 1995, pp. 477–482.
6. Nemat-Nasser, S. and Horii, H., Compression-induced nonplanar crack extension with application to splitting, exfoliation and rockburst. *J. Geophys. Res.*, 1982, **87**, 6805–6821.
7. Ashby, M. F. and Hallam, S. D., The failure of brittle solids containing small crack under compressive stress states. *Acta Metall.*, 1986, **34**, 497–510.
8. Atkinson, B. K., Introduction to fracture mechanics and its geophysical applications. In *Fracture Mechanics of Rock*. Ed. B. K. Atkinson, Academic Press, London, 1987, pp. 1–26.
9. McClintock, F. A. and Walsh, J. B., Friction of Griffith cracks in rocks under pressure. In *Proc. U.S. National Congress on Applied Mechanics*, 1962, 4th vol. II, pp. 1015–1021. American Society of Mechanical Engineers, New York.
10. Martin, C. D. and Chandler, N. A., The progressive fracture of Lac du Bonnet Granite. *Int. J. Rock Mech. Min. Sci. & Geomech. Abstr.*, 1994, **31**, 643–659.
11. Hatzor, Y. H., Zur, A. and Mimran, Y., Microstructure effects on micro-cracking and brittle failure of dolomites. *Tectonophysics*, 1997 (in press).
12. Tucker, M.E. and Wright, V. P., *Carbonate Sedimentology*. Blackwell Scientific Publications, 1990.
13. Brace, W. F., Paulding, B. W. and Scholz, C., Dilatancy in fracture of crystalline rocks. *J. Geophys. Res.*, 1966, **71**, 3939–3953.
14. Bieniawski, Z. T., Mechanism of brittle fracture of rock, Part II—experimental studies. *Int. J. Rock Mech. Min. Sci. & Geomech. Abstr.*, 1967, **4**, 407–423.
15. Atkinson, B. K. and Meredith, P. G., Experimental fracture mechanics data for rocks and minerals. In *Fracture Mechanics of Rock*, ed. B. K. Atkinson. Academic Press, London, 1987, pp. 477–526.
16. Gunsallus, K. L. and Kulhawy, F. H., A comparative evaluation of rock strength measures. *Int. J. Rock Mech. Min. Sci. & Geomech. Abstr.*, 1984, **21**, 233–248.
17. Griffith, A. A., The phenomena of rupture and flow in solids. *Phil. Trans Roy. Soc.*, 1921, **A221**, 163–197.
18. Kaplan, M. F., Crack propagation and fracture of concrete. *J. Am. Concrete Inst.*, 1961, **58**(5), 591–610.